AGU PUBLICATIONS

Geophysical Research Letters

RESEARCH LETTER
10.1002/2017GL075163

Key Points:
- We provide a uniform and comprehensive database of two decadal local shear wave splitting measurements in Southern California
- We identify several areas in Southern California where fast directions are significantly inconsistent with regional stress field
- Mechanisms other than regional stresses and active faults are needed to explain the upper crustal anisotropy in Southern California

Supporting Information:
- Supporting Information S1
- Data Set S1
- Data Set S2
- Data Set S3

Correspondence to:
Z. Li,
zefengli@gps.caltech.edu

Citation:
Li, Z., & Peng, Z. (2017). Stress- and structure-induced anisotropy in Southern California from two decades of shear wave splitting measurements. *Geophysical Research Letters*, *44*, 9607–9614. https://doi.org/10.1002/2017GL075163

Received 1 AUG 2017
Accepted 10 SEP 2017
Accepted article online 18 SEP 2017
Published online 5 OCT 2017

Stress- and Structure-Induced Anisotropy in Southern California From Two Decades of Shear Wave Splitting Measurements

Zefeng Li[1,2] **and Zhigang Peng**[1]

[1]School of Earth and Atmospheric Sciences, Georgia Institute of Technology, Atlanta, GA, USA, [2]Seismological Laboratory, California Institute of Technology, Pasadena, CA, USA

Abstract We measure shear wave splitting (SWS) parameters (i.e., fast direction and delay time) using 330,000 local earthquakes recorded by more than 400 stations of the Southern California Seismic Network (1995–2014). The resulting 232,000 SWS measurements (90,000 high-quality ones) provide a uniform and comprehensive database of local SWS measurements in Southern California. The fast directions at many stations are consistent with regional maximum compressional stress σ_{Hmax}. However, several regions show clear deviations from the σ_{Hmax} directions. These include linear sections along the San Andreas Fault and the Santa Ynez Fault, geological blocks NW to the Los Angeles Basin, regions around the San Jacinto Fault, the Peninsular Ranges near San Diego, and the Coso volcanic field. These complex patterns show that regional stresses and active faults cannot adequately explain the upper crustal anisotropy in Southern California. Other types of local structures, such as local rock types or tectonic features, also play significant roles.

1. Introduction

Seismic anisotropy in the upper crust can cause shear waves into two orthogonally polarized waves traveling at different velocities and arrive at slightly different times, a phenomenon generally called shear wave splitting (SWS). Crustal anisotropy can be explained by preferential opening of fluid-filled cracks under maximum horizontal compressive stress (σ_{Hmax}), also known as stress-induced anisotropy (Crampin et al., 1978; Leary et al., 1990; Nur & Simmons, 1969). However, studies associated with large strike-slip faults usually found that fast directions observed at near-fault stations were generally parallel to the local fault strike (e.g., Audet, 2014; Boness & Zoback, 2006; Cochran et al., 2003; Peng & Ben-Zion, 2004; Rasendra et al., 2014; Zhang & Schwartz, 1994). In addition, preferential mineral alignment, remnant features of paleostress, and sedimentary layering can also cause crustal anisotropy (Alford, 1986; Aster & Shearer, 1992; Sayers, 1994). Anisotropy associated with faults, mineral alignment, and sedimentation structures is generally categorized as structure-induced anisotropy. In some cases, due to different spatial sampling, a mixture of mechanisms on a single station can be observed (e.g., Cochran et al., 2003; Peng & Ben-Zion, 2004).

Southern California is an important region for SWS studies, mostly due to its structural complexity, highly active seismicity, and dense seismic instrumentation (Figure 1). Many SWS studies have been conducted in this region at various scales (Aster et al., 1990; Crampin et al., 1990; Li et al., 1994; Boness & Zoback, 2006; Li et al., 2015; Paulssen, 2004; Yang et al., 2011). These studies generally found that fast directions in Southern California are mainly controlled by regional stress, while some stations near major faults are controlled by fault structures. (e.g., Boness & Zoback, 2006). Li et al. (2015) observed varying fast directions across the San Jacinto Fault Zone, likely associated with heterogeneous rock damage from tectonic loading and earthquake rupture. However, these studies utilized different methods and data sets, resulting in heterogeneous SWS measurements. This may cause inconsistencies when comparing among different results.

In this paper we systematically measure SWS parameters of 330,000 local earthquakes recorded by Southern California Seismic Network (SCSN) in two decades (1995–2014). Our purpose is to provide a uniform and a complete database of local SWS measurements in Southern California. The measurements are obtained via fully automatic procedure and evaluated with quantitative criteria. Hence, our results are fully reproducible. The selected high-quality measurements are used to analyze spatial variations of shear wave anisotropy at local and regional scales. The patterns are then compared with σ_{Hmax} to identify regions with stress- or structure-induced anisotropy. Finally, we apply a spatial average method to obtain maps of anisotropy strength and fast direction in Southern California.

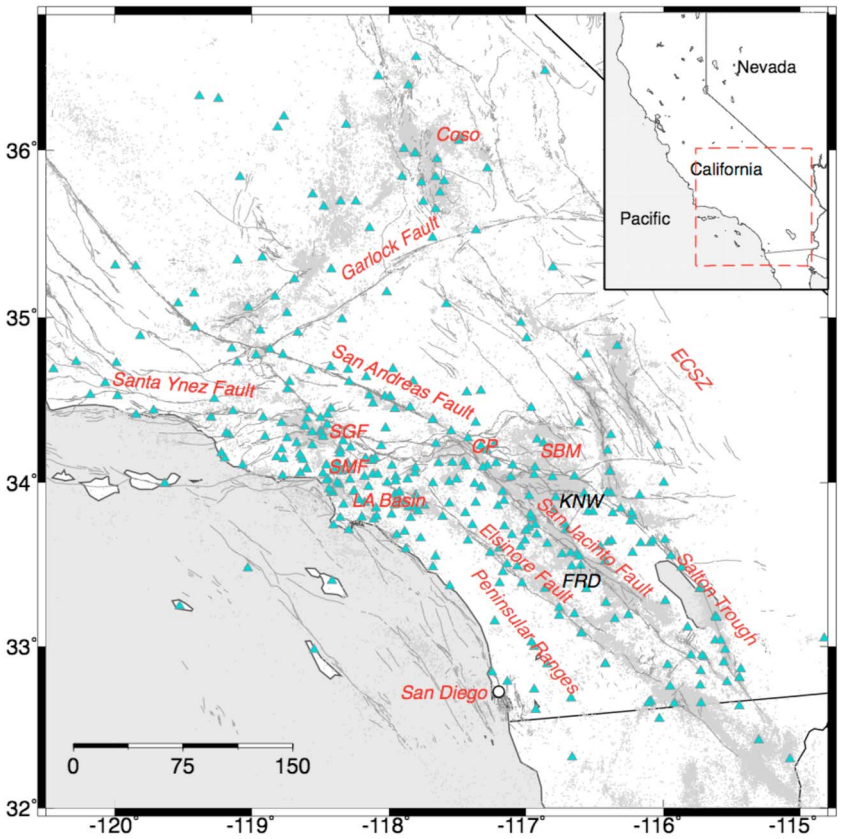

Figure 1. Seismicity (gray dots), the San Andreas Fault system (gray lines), and Southern California Seismic Network (cyan triangles). SGF: San Gabriel Fault, SMF: Santa Monica Fault, CP: Cajon Pass, SBM: Santa Bernardino Mountains, and ECSZ: eastern California shear zone. The inset marks the study region in a larger map of the western U.S.

2. Method and Data

Our automatic workflow is largely based on the work by Li et al. (2015), which involves several existing tools (Figure S1 in the supporting information). These include the Seismogram Transfer Program (STP, developed by Caltech), the Predict, Search, Invert, and Repeat (PSIR) phase picker to pick *S* arrivals (Li & Peng, 2016), and the MFAST code to measure SWS parameters (Savage et al., 2010). The waveform data are downloaded via STP, and the *S* phases are picked by the PSIR phase picker. The PSIR phase picker uses a "Predict, Search, Invert, and Repeat" procedure to search for abrupt changes on waveform amplitude around theoretical arrivals (Li & Peng, 2016). Fast directions and delay times are computed using the automated program MFAST (Savage et al., 2010). This code performs grid search over the fast direction-delay time (Φ-δt) space to minimize the energy on the component perpendicular to the initial polarization of shear waves (Silver & Chan, 1991). This process is applied with various shear wave windows, and cluster analysis is used to select the best solution from measurements of all windows (Teanby et al., 2004). An example of measurement on station KNW is shown in Figure S2.

The input data include 330,000 relocated local earthquakes recorded by the SCSN from 1995 to 2014 (Hauksson et al., 2012) (Figure 1). The SCSN consists of more than 400 stations (Figure 1). We choose the start year as 1995, because before that horizontal components were only available at a handful of stations. The events within the 45° cone beneath a station are examined (also known as the shear wave window), that is, the epicentral distance less than the hypocentral depth. This criterion is used to avoid *P*/*S* converted phases contaminating direct *S* phases (Booth & Crampin, 1985; Peng & Ben-Zion, 2004).

It is important to apply quality control to initial measurements in order to ensure robust subsequent analysis. We define high-quality measurements as follows: (1) average signal-to-noise ratio (SNR) of the *E* and *N* components >3, where SNR is defined as the ratio of root-mean-square amplitude 3 s after and before the

picked *S* arrival; (2) delay time $\delta t < 0.4$ s and δt error < 0.1 s; (3) fast direction Φ error $< 15°$; (4) cluster grade A and B (referring to Savage et al., 2010, for detailed definition); and (5) $20° <$ polarization angle of fast wave against incoming wave $<70°$ (Peng & Ben-Zion, 2004). These quantitative criteria are either empirical or inherited from previous studies (e.g., Peng & Ben-Zion, 2004; Savage et al., 2010). The use of quantitative criteria avoids subjective assessment and ensures that the obtained results are reproducible.

To obtain a first-order approximation of spatial variations in anisotropy, we apply a two-dimensional spatial averaging program TESSA to the resulting SWS measurements (Johnson et al., 2011). The program computes average anisotropy strength (defined as delay time per kilometer) and fast direction in 2-D grids. Hence, it does not account for depth dependency. We mesh the study area with a 5×5 km grid. The grids with more than 10 rays are considered to have relatively good resolution (Johnson et al., 2011). For each grid block, the fast directions are averaged in a circular statistical sense, if the standard deviation within that block is less than 30° and the standard error of the mean is less than 10° (Savage et al., 2016). The 2-D anisotropy strength inversion assumes that delay times accumulate along raypaths, which is a simplification of nonlinear relationship between apparent delay times and heterogeneous anisotropy strength. Therefore, the resulting map should be treated as first-order estimation of spatial anisotropy strength (Johnson et al., 2011).

3. Results

We end up with 232,000 SWS measurements (Table S1) with 90,000 high-quality ones (Table S2). We only use the high-quality measurements for the subsequent analyses. Before presenting the average results for all stations, we show individual measurements at stations KNW and FRD along the San Jacinto Fault to illustrate the stability of SWS measurements. For example, the individual measurements at station KNW remain nearly constant (albeit with some minor fluctuations) over two decades (Figure S3), indicating the stability of SWS measurement at this station. The average fast directions of 35° west of north (Figure S3) also agree well with previous studies (Aster et al., 1990; Crampin et al., 1990; Peacock et al., 1988; Yang et al., 2011). However, station FRD only 20 km away from KNW has different patterns when *M* 5 events occurred nearby (Figure S4). For example, two *M* 5 events occurred in 2001 and 2005 and the SWS parameters at station FRD are different from other time periods. Such temporal changes in SWS parameters could reflect changes in anisotropic parameters in the upper crust induced by these earthquakes (e.g., Liu et al., 2004), or more likely due to different spatial sampling with different earthquake locations (Peng & Ben-Zion, 2004). However, in this study we focus on spatial patterns and only examine general results averaged over two decades.

Figure 2a shows the rose diagrams of fast directions on each station. The fast directions on many stations are quasi-north, consistent with the regional σ_{Hmax} direction (Yang & Hauksson, 2013), while some near-fault stations display fault-parallel directions. In particular, some stations along the San Andreas Fault and the Elsinore Fault show clear fault-parallel directions. In the Los Angeles Basin (Figure 2b), the fast directions are about NNE, with weak rotation of fast directions from west to east. Stations near the Santa Monica Fault to north also show fault-parallel directions. However, the block in the north bounded by the Santa Monica Fault and the San Gabriel Fault (i.e., the San Fernando Valley and Simi Valley) shows approximately NNW direction with a few stations with mixed patterns.

The area near Cajon Pass, where the San Andreas Fault branches into the South San Andreas and the San Jacinto Faults, shows more complex patterns. Although fast directions can be still grouped spatially, these groups are not bounded by active faults or topographic features. Adjacent areas could have quite different fast directions. For example, the fast direction groups around the northern San Jacinto Fault and trifurcation area are perpendicular to the nearby groups, whose fast directions are parallel to the NW fault strike. These complexities may be associated with heterogeneous structures or complicate fault geometries in the area.

The average SWS parameters are computed for each station and compiled in Table S3. To better understand the SWS mechanisms in Southern California, we compare average fast directions with σ_{Hmax} derived from earthquake focal mechanisms (Yang & Hauksson, 2013) (Figure 3). As mentioned before, the preferential fast directions on most stations are consistent with the quasi-north σ_{Hmax} direction. Notable areas are the Los Angeles Basin, the vicinity of the Salton Sea, and the broad area NE to the Southern San Andreas Fault

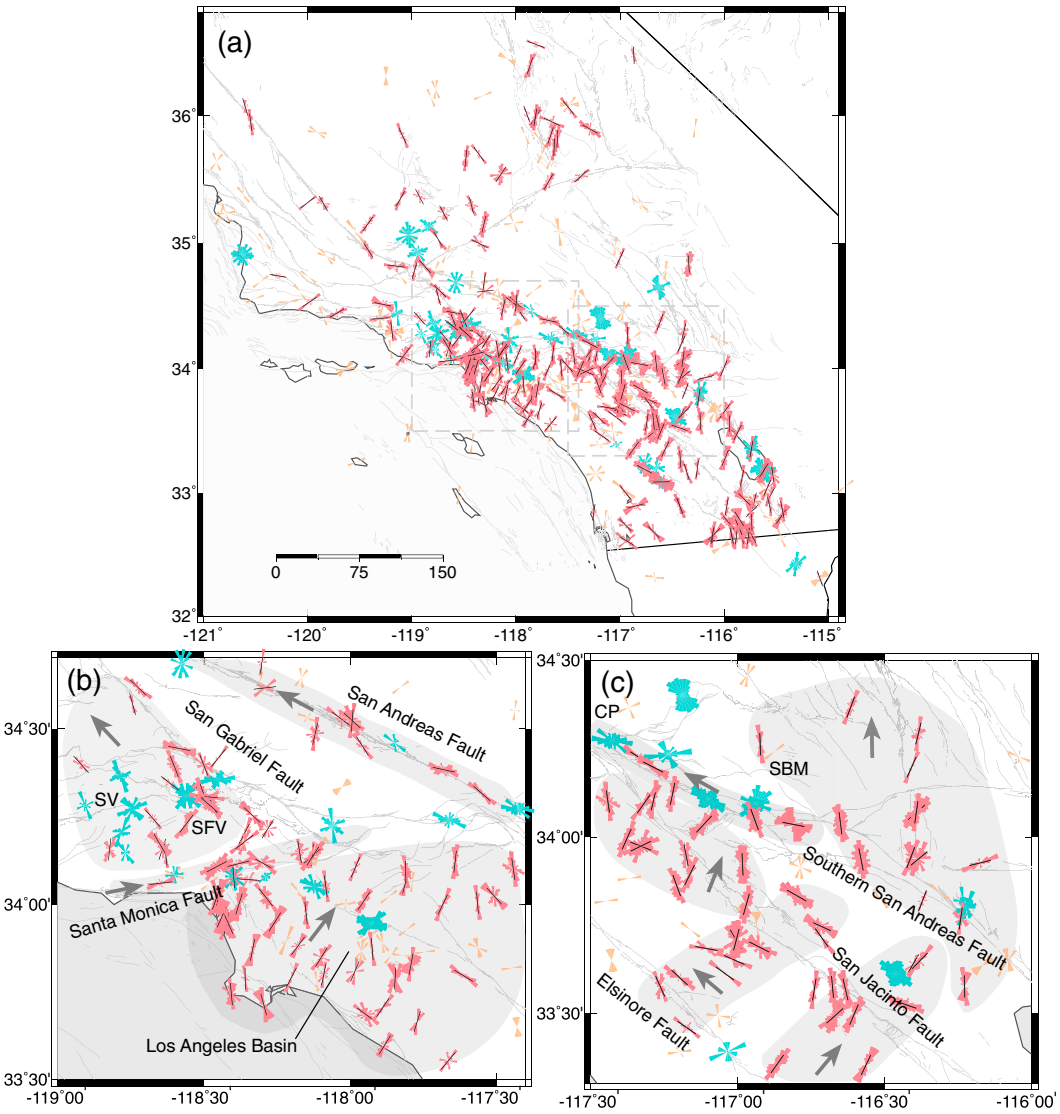

Figure 2. Rose diagrams of fast directions plotted on respective stations in Southern California. (a) Yellow diagrams are for stations with <10 measurements. Cyan diagrams are for stations with ≥10 measurements but resultant length < 0.25. The value 0.25 is an empirical threshold (e.g., Peng & Ben-Zion, 2004) below which the angular distribution is generally scattering or has mixed modes. Red diagrams are for stations with ≥10 measurements and resultant length > 0.25, suggesting clear preferential distribution. Dashed boxes mark the areas around the Los Angeles Basin and around the San Jacinto Fault, which are zoomed in further in Figures 2b and 2c. (b) Rose diagrams around the Los Angeles Basin. Similar and spatially close fast directions are grouped in shaded areas. The arrows represent the general directions in the groups. SV: Simi Valley and SFV: San Fernando Valley. (c) Rose diagrams around the San Jacinto Fault. The symbols are the same to those in Figure 2b. SBM: San Bernardino Mountains.

(Figure 3). However, several local areas have inconsistent directions between fast direction and σ_{Hmax}. From NW to SE, these areas include the Coso volcanic area, the San Andreas Fault, the Santa Ynez Fault, the block NW to the Los Angeles Basin, both sides of the San Jacinto Fault, and the southern end of Peninsular Ranges near San Diego.

Figure 4 shows the maps of spatial averaging fast directions and anisotropy strength. Similar to the observations above, the fast directions near major faults are parallel or subparallel to the fault strike (e.g., the San Andreas Fault, the San Jacinto Fault, the Elsinore Fault, the Santa Monica Fault, and the San Gabriel Fault). The areas with NNE fast directions include the Los Angeles Basin, the blocks along the San Jacinto Fault, and the NE side of the Southern San Andreas Fault (Figure 4a). We note a clear contrast of fast directions across the Southern San Andreas Fault. The NE side of the Southern San Andreas Fault shows NE

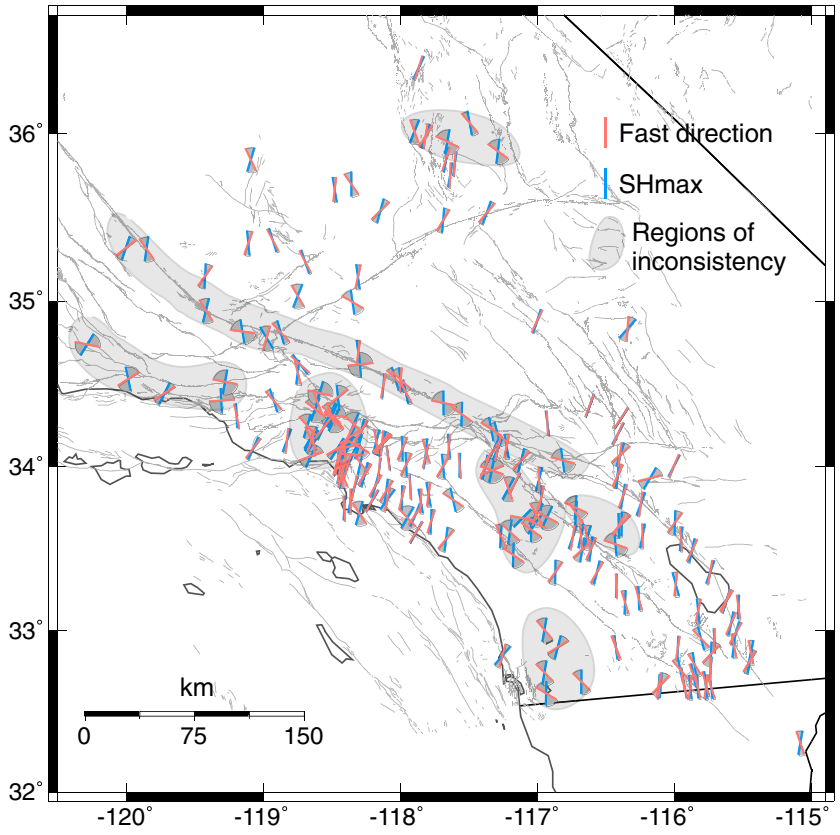

Figure 3. Comparison of average fast directions (red bars) and maximal horizontal compression stresses (σ_{Hmax}, blue bars) at all stations, which are extracted from focal mechanism analysis by Yang and Hauksson (2013). The angle difference between them is filled with black. Gray shaded areas mark major areas where fast directions are significantly different from σ_{Hmax}.

directions, while the SW side has NW directions (Figure 4a). In comparison with heterogeneous fast directions in this region, the anisotropy strength is relatively homogenous (Figure 4b). Within the areas with good data coverage, highly anisotropic bodies are observed around the Coso volcanic area and the southern Peninsular Ranges.

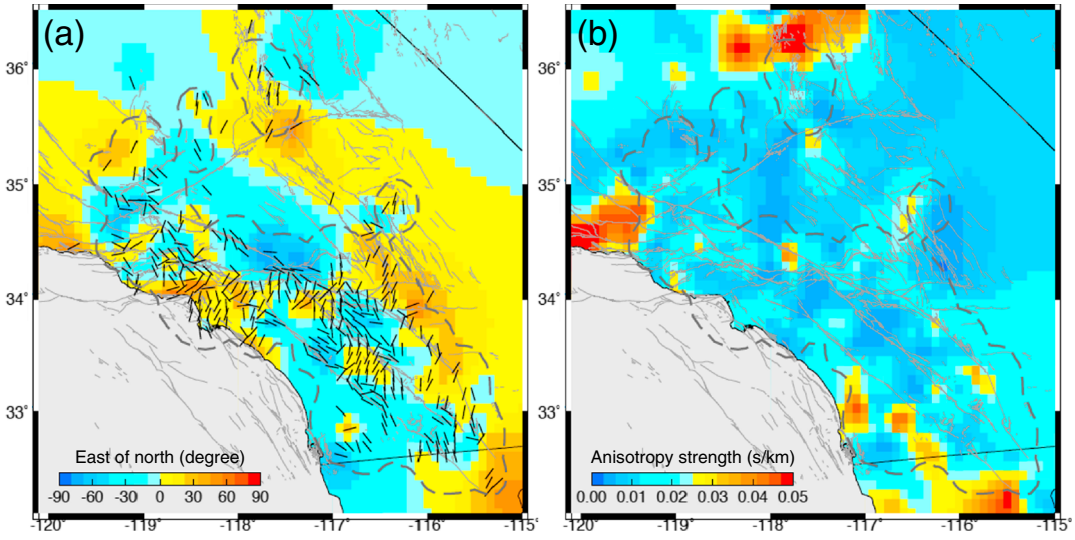

Figure 4. Spatial averaging of (a) fast directions and (b) anisotropy strength. The dashed contour surrounds the region with more than 10 measurements in each 5 × 5 km grid, which has relatively good resolution.

4. Discussions

Our SWS measurements from two decades of local earthquake data provide (as far as we know) the most complete SWS database in Southern California and are reproducible due to the automatic procedures and objective selection criteria. This SWS database could be a valuable resource for understanding physical mechanisms of crustal anisotropy and its relationship with regional σ_{Hmax} directions in Southern California (Figure 1). The general spatial patterns, as shown in Figure 2a, are highly heterogeneous, in stark contrast with the regional mantle anisotropy where *SKS* fast directions are consistently E-W region wide (e.g., Liu et al., 1995; Özalaybey & Savage, 1995; Polet & Kanamori, 2002). This indicates that the underlying mechanisms for crustal and mantle anisotropy are different. The local SWS observations show pervasive σ_{Hmax}- and fault-parallel fast directions (Figure 2a), which are consistent with previous studies (Boness & Zoback, 2006; Yang et al., 2011). However, close examination of the local-scale variations shows more complex patterns.

The Los Angeles Basin, for example, has NNE fast directions, which is consistent with σ_{Hmax} (Figures 2b and 3). In contrast, the northern block around the San Fernando Valley and Simi Valley shows NW directions, which are different from σ_{Hmax}. This suggests that fast directions can be controlled by local-scale geological blocks. A similar observation was reported by Okaya et al. (2016) showing that patterns of fast directions correlate with tectonic terranes across the Southern Central Range in Taiwan. They inferred that minerals in metamorphic rocks might form preferred alignment due to crustal deformation. Although the Los Angeles Basin and the northern block consist of similar sedimentary blocks, their internal deformation may differ as they belong to different geological regimes. The Los Angeles Basin is part of the Peninsular Ranges, while the northern block belongs to the Transverse Ranges.

As mentioned before, the area to the south of Cajon Pass shows the most complex patterns in the study region. Most of the fast directions are not σ_{Hmax} parallel (Figure 3) nor are fast direction groups bounded by active faults (Figure 2c). These observations indicate highly heterogeneous stress field and/or structures in the upper crust, coincident with the complicated fault geometry and mixture of sedimentary and granitic rocks observed at the surface (Figure S5). Similarly, Yang and Hauksson (2013) identified heterogeneous stress and a mixture of normal and strike-slip faulting styles in this area. Hence, we suggest that the fast direction distribution in this region partly reflects the combining complexity in structure, stress, and geology.

In Figure 3 we observed several areas with significant inconsistencies between fast directions and σ_{Hmax}, where localized structures are likely primary causes of shear wave anisotropy. However, the structures in effect may vary from place to place. Fault structures are one of the most dominant mechanisms. For example, the San Andreas Fault likely controls the crustal anisotropy in its vicinity. However, it is interesting that the fault-parallel directions terminate near the San Bernardino Mountains and the fast directions turn to become σ_{Hmax} parallel when approaching the Salton Sea. Such a change of patterns can be also observed in the stress field (Yang & Hauksson, 2013). This could be associated with the fault damage by the 1857 M_w 7.9 Fort Tejon earthquake, which stopped at the Cajon Pass and did not rupture the southernmost section of the San Andreas Fault. This inference is also consistent with previous observations of fault zone anisotropy induced by rock damage from large earthquake rupture (Li et al., 2014; Peng & Ben-Zion, 2004) but is inconsistent with a rapid healing in SWS parameters following the Kobe earthquake (Tadokoro et al., 1999).

Besides fault-related anisotropy, other structural mechanisms are likely prominent in Southern California, particularly in the block-shape areas where σ_{Hmax} and fast directions do not match. Around the Coso volcanic area, for example, local stress field may be perturbed by magma intrusion and migration within the lithosphere (Johnson et al., 2011; Shelley et al., 2014). In comparison, there are mixed granitic and sedimentary rocks near the San Jacinto Fault and the southern Peninsular Ranges (Figure S5). It is possible that the heterogeneities in lithological properties cause variations in fracture orientation under regional stress. Besides, minerals in granitic rocks might be aligned preferentially under crustal deformation (e.g., Okaya et al., 2016). However, definitive evidence from rock physics measurement on the outcrop samples in the region has not been available yet. These complex patterns revealed from our comprehensive data set demonstrate that regional stress and fault structures cannot adequately explain the upper crustal anisotropy in Southern California. Other mechanisms for crustal anisotropy (e.g., rock types, layering, etc.) could be more pervasive than was shown in previous studies (e.g., Boness & Zoback, 2006; Yang et al., 2011).

In this study we only focused on spatial variations of crustal anisotropy in Southern California. Detailed investigations on the depth distribution of anisotropy (e.g., Li et al., 2015; Peng & Ben-Zion, 2004) and temporal changes (e.g., Liu et al., 2004; Peng & Ben-Zion, 2005) are beyond the scope of this paper and will be the subject of subsequent work.

Acknowledgments
This research was supported by the Southern California Earthquake Center (SCEC contribution 7917). SCEC is funded by NSF Cooperative Agreement EAR-1033462 and USGS Cooperative Agreement G12 AC20038. All figures are made with the Generic Mapping Tools by Wessel et al. (2013). We thank Egill Hauksson and Martha Savage for answering various questions regarding the seismic data and the MFAST/TESSA code. The used seismic data are from the Data Center of the Southern California Seismic Network operated by Caltech/USGS.

References

Alford, R. M. (1986). Shear data in presence of azimuthal anisotropy: 56th *Annals International Meeting, Society Exploration Geophysics*, Expanded Abstract, 476–479. https://doi.org/10.1190/1.1893036

Aster, R. C., & Shearer, P. M. (1992). Initial shear wave particle motions and stress constraints at the Anza Seismic Network. *Geophysical Journal International*, *108*, 740–748.

Aster, R. C., Shearer, P. M., & Berger, J. (1990). Quantitative measurements of shear wave polarizations at the Anza seismic network, southern California: Implications for shear wave splitting and earthquake prediction. *Journal of Geophysical Research*, *95*, 12,449–12,473.

Audet, P. (2014). Layered crustal anisotropy around the San Andreas Faul near Parkfield, California. *Journal of Geophysical Research*, *120*, 3527–3543. https://doi.org/10.1002/2014JB011821

Boness, N., & Zoback, M. (2006). Mapping stress and structurally controlled crustal shear velocity anisotropy in California. *Geology*, *34*, 825–828.

Booth, D. C., & Crampin, S. (1985). Shear-wave polarizations on a curved wavefront at an isotropic free-surface. *Geophysical Journal of the Royal Astronomical Society*, *83*, 31–45.

Cochran, E. S., Vidale, J. E., & Li, Y.-G. (2003). Near-fault anisotropy following the Hector Mine earthquake. *Journal of Geophysical Research*, *108*(B9), 2436. https://doi.org/10.1029/2002JB002352

Crampin, S., Bamford, D., & Mcgonigle, R. (1978). Estimating crack parameters by inversion of *P* wave velocity-anisotropy. *Geophysical Journal of the Royal Astronomical Society*, *53*, 173–173.

Crampin, S., Booth, D. C., Evans, R., Peacock, S., & Fletcher, J. B. (1990). Change in shear wave splitting at Anza near the time of the North Palm Springs earthquake. *Journal of Geophysical Research*, *95*, 11,197–11,212.

Hauksson, E., Yang, W., & Shearer, P. M. (2012). Waveform relocated earthquake catalog for Southern California (1981 to June 2011). *Bulletin of the Seismological Society of America*, *102*(5), 2239–2244.

Johnson, J. H., M. K. Savage, and J. Townend (2011). Distinguishing between stress-induced and structural anisotropy at Mount Ruapehu Volcano, *New Zealand*. *Journal of Geophysical Research*, *116*, B12303. https://doi.org/10.1029/2011JB008308

Leary, P., Crampin, S., & McEvilly, T. (1990). Seismic fracture anisotropy in the Earth's crust—An overview. *Journal of Geophysical Research*, *95*, 11,105–11,114.

Li, Y. G., Teng, T. L., & Henyey, T. L. (1994). Shear-wave splitting observations in the northern Los Angeles Basin, California. *Bulletin of the Seismological Society of America*, *84*, 307–323.

Li, Z., & Peng, Z. (2016). An automatic phase picker for local earthquakes with predetermined locations: Combining a signal-to-noise ratio detector with 1D velocity model inversion. *Seismological Research Letters*, *87*(6), 1397–1405. https://doi.org/10.1785/0220160027

Li, Z., Peng, Z., Ben-Zion, Y., & Vernon, F. (2015). Spatial variations of shear-wave anisotropy near the San Jacinto Fault Zone in southern California. *Journal of Geophysical Research: Solid Earth*, *120*, 8334–8347. https://doi.org/10.1002/2015JB012483

Li, Z., Zhang, H., & Peng, Z. (2014). Structure-controlled seismic anisotropy along the Karadere–Düzce branch of the North Anatolian Fault revealed by shear-wave splitting tomography. *Earth and Planetary Science Letters*, *391*, 319–326.

Liu, H., Davis, P. M., & Gao, S. (1995). *SKS* splitting beneath southern California. *Geophysical Research Letters*, *22*, 767–770. https://doi.org/10.1029/95GL00487

Liu, Y., Teng, T.-L., & Ben-Zion, Y. (2004). Systematic analysis of shear-wave splitting in the aftershock zone of the 1999 Chi-Chi earthquake: shallow crustal anisotropy and lack of precursory variations. *Bulletin of the Seismological Society of America*, *94*, 2330–2347.

Nur, A., & Simmons, G. (1969). Stress-induced velocity anisotropy in rock: An experimental study. *Journal of Geophysical Research*, *74*, 6667–6674.

Okaya, D., Christensen, N. I., Ross, Z. E., & Wu, F. T. (2016). Terrane-controlled crustal shear wave splitting in Taiwan. *Geophysical Research Letters*, *43*, 556–563. https://doi.org/10.1002/2015GL066446

Özalaybey, S., & Savage, M. K. (1995). Shear-wave splitting beneath western United States in relation to plate tectonics. *Journal of Geophysical Research*, *100*, 18,135–18,149. https://doi.org/10.1029/95JB00715

Paulssen, H. (2004). Crustal anisotropy in southern California from local earthquake data. *Geophysical Research Letters*, *31*, L01601. https://doi.org/10.1029/2003GL018654

Peacock, S., Crampin, S., Booth, D. C., & Fletcher, J. B. (1988). Shear-wave splitting in the Anza seismic gap southern California: temporal variations as possible precursors. *Journal of Geophysical Research*, *93*, 3339–3356.

Peng, Z., & Ben-Zion, Y. (2004). Systematic analysis of crustal anisotropy along the Karadere-Düzce branch of the North Anatolian fault. *Geophysical Journal International*, *159*, 253–274. https://doi.org/10.1111/j.1365-246X.2004.02379.x

Peng, Z., & Ben-Zion, Y. (2005). Spatio-temporal variations of crustal anisotropy from similar events in aftershocks of the 1999 *M* 7.4 İzmit and *M* 7.1 Duzce, Turkey, earthquake sequences. *Geophysical Journal International*, *160*, 1027–1043. https://doi.org/10.1111/j.1365-246X.2004.02379.x

Polet, J., & Kanamori, H. (2002). Anisotropy beneath California: Shear wave splitting measurements using a dense broadband array. *Geophysical Journal International*, *149*, 313–327. https://doi.org/10.1046/j.1365-246X.2002.01630.x

Rasendra, N., Bonnin, M., Mazzotti, S., & Tiberi, C. (2014). Crustal and upper mantle anisotropy related to fossilized transpression fabric along the Denali Fault, northern Canadian Cordillera. *Bulletin of the Seismological Society of America*, *104*(4), 1964–1975. https://doi.org/10.1785/0120130233

Savage, M. K., Aoki, Y., Unglert, K., Ohkura, T., Umakoshi, K., Shimizu, H., … Mori, J. (2016). Stress, strain rate and anisotropy in Kyushu, Japan. *Earth and Planetary Science Letters*, *439*, 129–142.

Savage, M. K., A. Wessel, N. Teanby, and T. Hurst (2010). Automatic measurement of shear wave splitting and applications to time varying anisotropy at Mt. Ruapehu volcano, New Zealand, *Journal of Geophysical Research*, *115*, B12321. https://doi.org/10.1029/2010JB007722

Sayers, C. M. (1994). The elastic anisotropy of shales. *Journal of Geophysical Research*, *99*, 767–774.

Shelley, A., Savage, M., Williams, C., Aoki, Y., & Gurevich, B. (2014). Modeling shear wave splitting due to stress-induced anisotropy, with an application to Mount Asama Volcano, Japan. *Journal of Geophysical Research: Solid Earth*, *119*, 4269–4286. https://doi.org/10.1002/2013JB010817

Silver, P., & Chan, W. (1991). Shear-wave splitting and subcontinental mantle deformation. *Journal of Geophysical Research*, *96*, 16,429–16,454.
Tadokoro, K., Ando, M., & Umeda, Y. (1999). Swave splitting in the aftershock region of the 1995 Hyogo-ken Nanbu earthquake. *Journal of Geophysical Research*, *104*, 981–991.
Teanby, N., Kendall, J., & Van der Baan, M. (2004). Automation of shear-wave splitting measurements using cluster analysis. *Bulletin of the Seismological Society of America*, *94*, 453–463.
Wessel, P., Smith, W. H. F., Scharroo, R., Luis, J. F., & Wobbe, F. (2013). Generic Mapping Tools: Improved version released. *Eos, Transactions, American Geophysical Union*, *94*, 409–410. https://doi.org/10.1002/2013EO450001
Yang, W., & Hauksson, E. (2013). The tectonic crustal stress field and style of faulting along the Pacific North America Plate boundary in Southern California. *Geophysical Journal International*, *194*(1), 100–117. https://doi.org/10.1093/gji/ggt113
Yang, Z., Sheehan, A., & Shearer, P. (2011). Stress induced upper crustal anisotropy in southern California, *Journal of Geophysical Research*, *116*, B02302. https://doi.org/10.1029/2010JB007655
Zhang, Z., & Schwartz, S. Y. (1994). Seismic anisotropy in the shallow crust of the Loma Prieta segment of the San Andreas fault system. *Journal of Geophysical Research*, *99*, 9651–9661.